# Hydroxylamine Seeding of Colloidal Au Nanoparticles. 3. Controlled Formation of Conductive Au Films

Kenneth R. Brown, L. Andrew Lyon, Audrey P. Fox, Brian D. Reiss, and Michael J. Natan*

*Department of Chemistry, The Pennsylvania State University, 152 Davey Laboratory, University Park, Pennsylvania 16802-6300*

*Received February 3, 1998. Revised Manuscript Received October 13, 1999*

An approach to enlarge preformed colloidal Au nanoparticles in solution based on the Au colloidal surface-catalyzed reduction of $Au^{3+}$ by $NH_2OH$ ("seeding") has been adapted to 12-nm-diameter colloidal Au nanoparticles immobilized in monolayers and multilayers. Bulk characterization of the ensuing films was carried out by atomic absorption, UV−vis−near-IR optical spectroscopy, cyclic voltammetry, and dc resistance measurements. Exposure of a 12-nm-diameter Au colloid monolayer on organosilane-modified glass surfaces to $NH_2OH$/$Au^{3+}$ leads to rapid particle growth and coalescence: after roughly 5−10 min, the optical and electrical properties closely resemble that of conductive Au thin films prepared by evaporation. Evolution of the nanometer-scale architecture was followed using atomic force microscopy (AFM), surface-enhanced Raman scattering (SERS), surface plasmon resonance (SPR), and field emission scanning electron microscopy (FE-SEM), leading to the following key findings: (i) Seeding of surface-confined colloidal Au leads to a very different distribution in particle size/shape than seeding with identical particles in solution. (ii) $Au^{3+}$/$NH_2OH$-mediated growth of surface-confined colloidal Au is highly dependent on particle coverage, with different particle densities in monolayers leading to distinct film architectures that are easily detected by FE-SEM and SPR.

## Introduction

We describe herein the preparation and characterization of conductive Au films prepared by controlled growth of the nanoparticles in Au colloid monolayers and multilayers using aqueous solutions of $NH_2OH$/$HAuCl_4$. Formation of conductive metal films by faradaic and nonfaradaic deposition onto immobilized metal nanoparticles is a widely used process in industry,[1] and of significant recent interest in academia.[2−4] The focus of this work has typically been on production of thin films exhibiting high conductivity and good adhesion, with special attention given to micrometer-to-sub-micrometer control of film thickness and ease of fabrication. Although largely successful, two aspects of film growth by electroless metal deposition have received little attention. The first is that the number of metal nanoparticles used to nucleate film growth is usually not a controllable parameter. As a result, detailed mechanistic information about particle coalescence is lacking. The second is that the analogous processes in solution—that is, enlargement of suspended metal nanoparticles—have not been studied. Accordingly, information about the size and shape of growing particles is unavailable.

In the previous paper, we described how suspensions of large (>50 nm diameter) Au nanoparticles could be prepared by seeding of preformed, 12-nm-diameter colloidal Au solutions with $Au^{3+}$ and $NH_2OH$.[5] The kinetics for $NH_2OH$ reduction of adsorbed $Au^{3+}$ greatly exceeds the rate of solution reduction,[6] preventing nucleation of new particles. Instead, two distinct particle populations were formed, with ∼90% of the particles being extremely spherical—in fact, more spherical than any previously described direct syntheses of large particles[7]—and ∼10% of the particles being high-aspect ratio colloidal Au rods, also novel in that deliberate synthetic routes to such particles have not been reported.

* Author whom all correspondence should be addressed via e-mail at natan@chem.psu.edu.

(1) (a) Mallory, G. O.; Hajdu, J. B., Ed. *Electroless Plating: Fundamentals & Applications*; American Electroplaters and Surface Finishers Society: Orlando, FL, 1990. (b) Sullivan, A. M.; Kohl, P. A. *J. Electrochem. Soc.* **1995**, *142*, 2250−2255. (c) Romankiw, L. T.; Turner, D. R., Eds. *Electrodeposition Technology: Theory and Practice*; The Electrochemical Society: Pennington, NJ, 1987.

(2) (a) Dressick, W. J.; Dulcey, C. S.; Georger, J. H., Jr.; Calabese, G. S.; Calvert, J. M. *J. Electrochem. Soc.* **1994**, *141*, 210−220. (b) Calvert, J. M.; Dressick, W. J.; Dulcey, C. S.; Chen, M. S.; Georger, J. H.; Stenger, D. A.; Koloski, T. S.; Calabrese, G. S. In *Polymers for Microelectronics: Resists and Dielectrics*; Thompson, L. F., Willson, C. G., Tagawa, S., Eds.; Advances in Chemistry 537; American Chemical Society: Washington, DC, 1994; Chapter 14.

(3) (a) Eliadis, E. D.; Nuzzo, R. G.; Gerwirth, A. A.; Alkire, R. C. *J. Electrochem. Soc.* **1997**, *144*, 96−105. (b) Lin, W.; Wiegand, B. C.; Nuzzo, R. G.; Girolami, G. S. *J. Am. Chem. Soc.* **1996**, *118*, 5977−5987. (c) Lin, W.; Nuzzo, R. G.; Girolami, G. S. *J. Am. Chem. Soc.* **1996**, *118*, 5988−5996. (d) Moberg, P.; McCarley, R. L. *J. Electrochem. Soc.* **1997**, *144*, L151−L153. (e) Hidber, P. C.; Helbig, W.; Kim, E.; Whitesides, G. M. *Langmuir* **1996**, *12*, 1375−1380.

(4) Bradley, J. C.; Crawford, J.; Ernazarova, K.; McGee, M.; Stephens, S. G. *Adv. Mater.* **1997**, *9*, 1168−1171.

(5) Brown, K. R.; Walter, D. G.; Natan, M. J. Chem. Mater. **2000**, *12*, 306−313 (previous paper in this journal).

(6) Stremsdoerfer, G.; Perrot, H.; Martin, J. R.; Clechet, P. *J. Electrochem. Soc.* **1988**, *135*, 2881−2885.

10.1021/cm980066h CCC: $19.00 
Published on Web 12/29/1999

Armed with detailed knowledge about the properties of $NH_2OH$-based Au enlargement of 12-nm-diameter colloidal Au in solution, we have investigated the same reaction for immobilized Au colloid monolayers[8−10] and multilayers,[11,12] with three synthetic goals: (i) Theory predicts that large-diameter colloidal Au particles are more active for surface enhanced Raman scattering (SERS)[13] than smaller ones.[14] However, in our approach to SERS-active substrates based on self-assembly colloidal Au or Ag particles from solution, only low concentrations of large Au nanoparticles can be stably prepared, and the diffusion coefficient is inversely proportional to the particle radius.[15] Thus, manufacture of SERS substrates by self-assembly of, say, 50-nm-diameter colloidal Au particles is laborious. (ii) The insulator−conductor transition[16] in discontinuous or semicontinuous Au thin films prepared by evaporation is of fundamental interest and has been investigated continuously for almost 20 years.[17] Unfortunately, evaporation affords little control of structure on the nanometer scale, and we reasoned that controlled enlargement of a two-dimensional (2-D) array of single-sized Au nanoparticles might lead to well-defined 2-D conductors. (iii) Finally, we wished to explore the prospects for solution fabrication of thin Au films well-suited for surface plasmon resonance (SPR).[18] Detection of biomolecular complex formation and/or dissociation using SPR is becoming increasingly common.[19] The phenomenon is based on changes in reflectivity of ∼50-nm-diameter Au films coated with 200-nm-thick films of carboxylated dextrans.[20] However, the inconvenience and expense associated with mass production of evaporated thin Au films with such narrowly defined specifications argues against their use in high-throughput screening,[21] a data-intensive route to discovery of new pharmaceutical leads.

We find that $NH_2OH$-mediated reduction of $Au^{3+}$ is an excellent route to enlargement of immobilized 12-nm-diameter colloidal Au nanoparticles tethered to organosilane-coated glass substrates. By using low concentrations of $Au^{3+}$ (added as $HAuCl_4$), it is possible to monitor and control the rate of particle growth and coalescence. Immersion of Au colloid monolayers for just a few minutes into a shaken flask containing 0.01% $HAuCl_4$/0.4 mM $NH_2OH$ leads to evolution of optical properties very similar to those of evaporated Au films near the insulator−conductor threshold; additional exposure leads to metallic thin films with dc resistances as low as 1−10 Ω, allowing them to be used for cyclic voltammetric measurements. Investigation of film nanostructure using atomic force microscopy (AFM) and field-emission scanning electron microscopy (FE-SEM) indicates that enlarged particles are neither spherical nor cylindrical, but rather highly complex in shape. Not surprisingly, $NH_2OH$-mediated particle enlargement leads to dramatic improvements in SERS enhancement factors. We also show that the nanoscale morphology of conductive films depends critically on the initial coverage of 12-nm-diameter Au nanoparticles, and that SPR measurements are acutely sensitive to such differences, even in films exhibiting ostensibly identical bulk optical and electrical properties.

## Experimental Section

**Materials.** $Na_2SO_4$, *trans*-4,4′-bis(4-pyridyl)ethylene (BPE), 2-mercaptoethylamine, and trisodium citrate were purchased from Aldrich. $NH_2OH{\cdot}HCl$ (henceforth $NH_2OH$) and hydrogen tetrachloroaurate ($HAuCl_4$) were purchased from Acros. $[Ru(NH_3)_6]Cl_3$ was obtained from Strem Chemicals. 3-aminopropyltrimethoxysilane (APTMS) and 3-mercaptopropyltrimethoxysilane (MPTMS) were purchased from United Chemical Technologies. HCl, $HNO_3$, $H_2SO_4$, and $H_2O_2$ were obtained from VWR or Fisher Scientific. $H_2O$ was purified to >18 MΩ with a Barnstead Nanopure water purification system. All chemicals were used as received except for BPE, which was recrystallized several times from $CH_3OH/H_2O$. Glass substrates (microscope slides and coverslips) were obtained from VWR and cleaned, using previously described protocols, prior to derivatization.[22]

(7) (a) Hayat, M. A., Ed. *Colloidal Gold: Principles, Methods, and Applications*; Academic Press: San Diego, 1989; Vols. 1 and 2. (b) Frens, G. *Nature* **1972**, *241*, 20−22. (c) Frens, G. *Kolloid-Z. u. Z. Polymere* **1972**, *250*, 736−741. (d) Goodman, S. L.; Hodges, G. M.; Trejdosiewicz, L. K.; Livingston, D. C. *J. Microsc.* **1981**, *123*, 201−213.

(8) (a) Freeman, R. G.; Grabar, K. C.; Allison, K. J.; Bright, R. M.; Davis, J. A.; Guthrie, A. P.; Hommer, M. B.; Jackson, M. A.; Smith, P. C.; Walter, D. G. Natan, M. J. *Science* **1995**, *267*, 1629−1632. (b) Grabar, K. C.; Freeman, R. G.; Hommer, M. B.; Natan, M. J. *Anal. Chem.* **1995**, *67*, 735−743.

(9) Doron, A.; Katz, E. Willner, I. *Langmuir* **1995**, *11*, 1313−1317.

(10) Giersig, M.; Mulvaney, P. *Langmuir* **1993**, *9*, 3408−3413. (b) Sato, T.; Hasko, D. G.; Ahmed, H. *J. Vac. Sci. Technol. B* **1997**, *15*, 45−48.

(11) Musick, M. D.; Keating, C. D.; Keefe, M. H.; Natan, M. J. *Chem. Mater.* **1997**, *9*, 1499−1501.

(12) (a) Brust, M.; Walker, M.; Bethell, D.; Schiffrin, D. J.; Whyman, R. *J. Chem. Soc., Chem. Commun.* **1994**, 801−802. (b) Terrill, R. H.; Postlewaite, T. A.; Chen, C.-H.; Poon, C. C.; Terzis, A.; Chen, A.; Hutchison, J. E.; Clark, M. R.; Wignall, G.; Londono, J. D.; Superfine, R.; Falvo, M.; Johnson, C. S., Jr.; Samulski, E. T.; Murray, R. W. *J. Am. Chem. Soc.* **1995**, *117*, 12537−12548. (c) Hostetler, M. J.; Murray, R. W. *Curr. Opin. Colloid Interface Sci.* **1997**, *2*, 42−50.

(13) (a) Brandt, E. S.; Cotton, T. M. In *Investigations of Surfaces and Interfaces, Part B*, 2nd ed.; Rossiter, B. W., Baetzold, R. C., Eds.; John Wiley & Sons: NewYork, 1993; Vol. IXB, Chapter 8, pp 663−718. (b) Creighton, J. A. In *Surface Analysis Techniques and Applications*; Neagle, W., Randell, D. R., Eds.; Royal Society of Chemistry: Cambridge, 1990; pp 13−26. (c) Cotton, T. M.; Kim, J.-H.; Chumanov, G. D. *J. Raman Spectrosc.* **1991**, *20*, 729−42. (d) Garrell, R. L. *Anal. Chem.* **1989**, *61*, 401A−411A.

(14) Zeman, E. J.; Schatz, G. C. *J. Phys. Chem.* **1987**, *91*, 634−643.

(15) Grabar, K. C.; Smith, P. C.; Musick, M. D.; Davis, J. A.; Walter, D. G.; Jackson, M. A.; Guthrie, A. P.; Natan, M. J. *J. Am. Chem. Soc.* **1996**, *118*, 1148−1152.

(16) (a) Clerc, J. P.; Giraud, G.; Laugier, J. M.; Luck, J. M. *Adv. Phys.* **1990**, *39*, 191−309.

(17) (a) Brouers, F.; Clerc, J. P.; Giraud, G.; Laugier, J. M.; Randriamantany, Z. A. *Phys. Rev. B* **1993**, *47*, 666−673. (b) Stefanou, N.; Modinos, A. *J. Phys.: Condens. Matter* **1991**, *3*, 8149−8157. (c) Yagil, Y.; Gadenne, P.; Julien, C.; Deutscher, G. *Phys. Rev. B* **1992**, *46*, 2503−2511. (d) Abeles, B.; Sheng, P.; Coutts, M. D.; Arie, Y. *Adv. Phys.* **1975**, *24*, 407−461. (e) Sheng, P.; Sichel, E. K.; Gittleman, J. I. *Phys. Rev. Lett.* **1978**, *40*, 1197−1200. (f) Grannan, D. M.; Garland, J. C.; Tanner, D. B. *Phys. Rev. Lett.* **1981**, *46*, 375−378. (g) Hundley, M. F.; Zettl, A. *Phys. Rev. B* **1988**, *38*, 10290−10296.

(18) (a) Raether, H. *Surface Plasmons*; Springer-Verlag: Berlin, 1988. (b) Sambles, J. R.; Bradbury, G. W.; Yang, F. *Contemporary Phys.* **1991**, *32*, 173−183.

(19) (a) Barbas, S. M.; Ditzel, H. J.; Salonen, E. M.; Yang, W.-P.; Silverman, G. J.; Burton, D. R. *Proc. Natl. Acad. Sci. U.S.A.* **1995**, *92*, 2529−2533. (b) Ladbury, J. E.; Lemmon, M. A.; Zhou, M.; Green, J.; Botfield, M. C.; Schlessinger, J. *Proc. Natl. Acad. Sci. U.S.A.* **1995**, *92*, 3199−3203. (c) Plant, A. L.; Brigham-Burke, M.; Petrella, E. C.; O'Shannessy, D. J. *Anal. Biochem.* **1995**, *226*, 342−348. (d) Salamon, Z.; Tollin, G. *Biophys. J.* **1996**, *71*, 848−857. (e) Ward, L. D.; Howlett, G. J.; Hammacher, A.; Weinstock, J.; Yasukawa, K.; Simpson, R. J.; Winzor, D. J. *Biochemistry* **1995**, *34*, 2901−2907. (f) Xu, J.; Wu, D.; Slepak, V. Z.; Simon, M. I. *Proc. Natl. Acad. Sci. U.S.A.* **1995**, *92*, 2086−2090. (g) Frey, B. L.; Jordon, C. E.; Kornguth, S.; Corn, R. M. *Anal. Chem.* **1995**, *67*, 4452−4457.

(20) Yeung, D.; Gill, A.; Maule, C. H.; Davies, R. J. *Trends Anal. Chem.* **1995**, *14*, 49−56.

(21) Gordon, E. M.; Barret, R. W.; Dower, W. J.; Fodor, S. P. A.; Gallop, M. A. *J. Med. Chem.* **1994**, *37*, 1385−1401.

**Film Growth.** Colloidal Au nanoparticles measuring 12 ± 1 nm in diameter were prepared, sized by TEM/image analysis, and assembled into 2-D arrays on silanized glass substrates according to previously described methods.[8] Au colloid multilayers were made by taking 12-nm-diameter colloidal Au monolayers (immobilized on MPTMS-coated glass) and immersing them for 10 min in 10 mM 2-mercaptoethylamine. After exhaustive rinsing with $H_2O$, the surfaces were immersed in a fresh solution of 17 nM, 12-nm-diameter colloidal Au nanoparticles for 1 h. This process was repeated between 3 and 8 times (as indicated in the text).

In brief, hydroxylamine-reduced Au metal films were developed on colloidal monolayers in 600 mL of 0.01% $HAuCl_4$/0.4 mM $NH_2OH$ on an orbital shaker. The surfaces were dried for optical spectra, conductivity measurements, AFM, FE-SEM, and atomic absorbance.

More specifically, reduced Au metal films started from sets of Au colloid monolayers were prepared using either glass microscope slides (cut to 2.5 × 0.8 cm) or glass microscope coverslips (2.5 × 2.5 cm). One side was wiped clean of colloid and the optical spectra were taken of the surface immersed in water. All monolayers were transferred to a solution of $NH_2OH$ in an 8 in. × 8 in. Pyrex dish and placed on a Lab-Line orbital shaker operated at 120 rpm. A solution of $HAuCl_4$ was added to initiate the reaction. All surfaces were exposed to the same reducing solution; samples were removed at regular intervals for subsequent characterization. After removal, surfaces were immediately washed in water, dried in a stream of Ar gas and stored in vials or Petri dishes. For each surface, an optical spectrum was recorded, after which two electrical contacts were deposited using a Circuit Works conductive pen from Planned Products. When the contacts dried, resistance between the contacts was measured and then the surfaces were imaged by AFM. At least two 5 $\mu$m × 5 $\mu$m scans and eight 1 $\mu$m × 1 $\mu$m images were collected from each surface; for FE-SEM, two 5 $\mu$m scans and two 1 $\mu$m scans were taken for each surface.

Atomic absorption experiments were carried out as follows. Metallic Au was removed from the area bounded by a 0.6-cm-diameter O-ring by mixing 50 $\mu$L of concentrated HCl and 50 $\mu$L of concentrated $HNO_3$ in situ. $H_2O$ was added after the Au film had dissolved and was placed in a volumetric flask. The surface was then rinsed copiously with $H_2O$ and all rinses were pooled with the acid to a final volume of 10 mL.

**Instrumentation.** Optical spectra were acquired on either an HP8452 UV−vis connected to a Swan 386 (IBM compatible) or a Perkin-Elmer Lambda 9 spectrophotometer connected to a Gateway 486 (IBM compatible), using software supplied by the manufacturer. Resistance measurements were made with a Fluke 77 multimeter. Atomic absorbance measurements were made using a Perkin-Elmer 1100B Graphite Furnace atomic absorption spectrophotometer.

SERS spectra were also collected using a Detection Limited microRaman system which consists of a Solution 633 helium−neon laser with a distal probe connected by fiber optic cable. The CCD and data collection were controlled by a Monorail PC clone running DLSPEC software. The lens used had a working distance of 3 mm, resulting in a spot size of ~5 $\mu$m. The band-pass for the microRaman system is ~8 $cm^{-1}$. Data were processed and analyzed using GRAMS 32 software. Spectra were collected at 632.8 nm. All samples were run at 23 mW with 10-s integration time.

AFM images were acquired using a Digital Instruments Nanoscope IIIa in tapping mode at a frequency of 1−2 Hz, and 512 lines per image using standard Si cantilevers from Digital Instruments. TEM images were taken in a JEOL model 1200EXII operated at 80 kV accelerating voltage and 100K magnification. FE-SEM images were acquired on a JEOL JSM 6320F at 3.0 kV accelerating voltage and 100K magnification.

**Scheme 1. Enlargement of Au Colloid Monolayers by $NH_2OH$ Seeding**

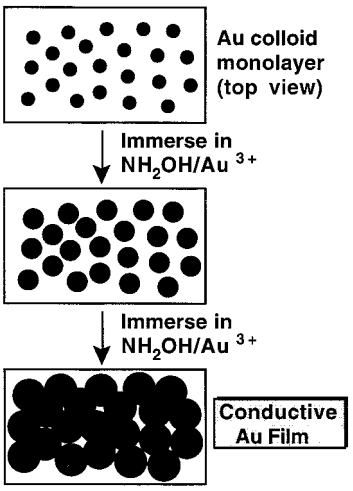


SPR spectra were obtained on surfaces of dimensions 2.5 × 2.5 cm with a hemispherical prism (index of refraction = 1.515) illuminated by a Spectra-Physics model 127 HeNe gas laser. Data were collected with a Newport photodiode (1-ns rise time) and a Stanford Research optical chopper and 530 lock-in amplifier. The instrument was operated by in-house written Labview 4.0 software operated by a Power Computing PowerCenter 150.

All electrochemical measurements were carried out using a PAR model 273A potentiostat/Galvanostat operated with model 270 Software on a Gateway 486 IBM-compatible computer. All electrochemical measurements were taken in a beaker with the working electrode hanging in solution. Electrochemical solutions consisted of 5 mM $[Ru(NH_3)_6]Cl_3$ in 0.1 M $Na_2SO_4$. The sample was scanned four times with the fourth scan being saved.

## Results and Discussion

**Bulk Optical and Electrical Properties.** On the basis of our results on seeding of colloidal Au nanoparticles with $Au^{3+}/NH_2OH$ in solution, we anticipated that enlargement of surface-confined particles to proceed as shown in Scheme 1. Starting with a Au colloid monolayer with ~20% of close-packing coverage, immersion into the seeding solution should lead to particle growth. It is expected that the particles will not move (a consequence of several hundred bonds between colloidal Au surface and either $-NH_2$ or $-SH$ groups on the organosilane),[8] and hoped that (at least at early stages of growth), the particles will retain their spherical character.

Figure 1 shows visible optical spectra over time for a 12-nm Au colloid monolayer on APTMS-coated glass substrate upon immersion in a solution of 0.01% $HAuCl_4$/4 mM $NH_2OH$.[23] Every 10 s for the first minute (top panel), the absorbance continually increases from the initial colloidal Au monolayer (a). In this time frame there is a noticeable increase in total absorbance but the spectral peak near 520 nm is still clearly defined, albeit slightly red-shifted. As previously discussed,[5] the increased extinction and the shift of $\lambda_{max}$ to longer wavelengths are both consistent with increased dimen-

(22) Grabar, K. C.; Allison, K. J.; Baker, B. E.; Bright, R. M.; Brown, K. R.; Freeman, R. G.; Fox, A. P.; Keating, C. D.; Musick, M. D.; Natan, M. J. *Langmuir* **1996**, *12*, 2353−2361.

(23) In contrast to all subsequent experiments, which were carried out in an orbital shaker to ensure good reagent delivery to the surface, the experiments in Figure 1 were carried out directly in UV−vis cuvettes, with no stirring beyond the initial addition of reagents.

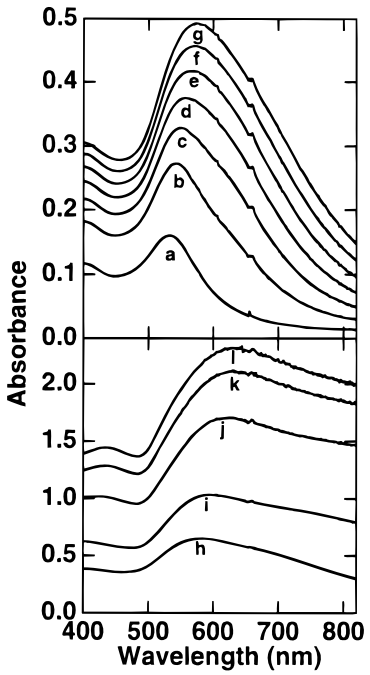


**Figure 1.** Optical spectra in $H_2O$ of a 12-nm-diameter Au colloid monolayer on APTMS-coated glass as prepared (a), and after immersion in 0.01% $HAuCl_4$/4 mM $NH_2OH$ for 10 (b), 20 (c), 30 (d), 40 (e), 50 (f), 60 (g), 120 (h), 300 (i), 900 (j), 1500 (k), and 2700 s (l).

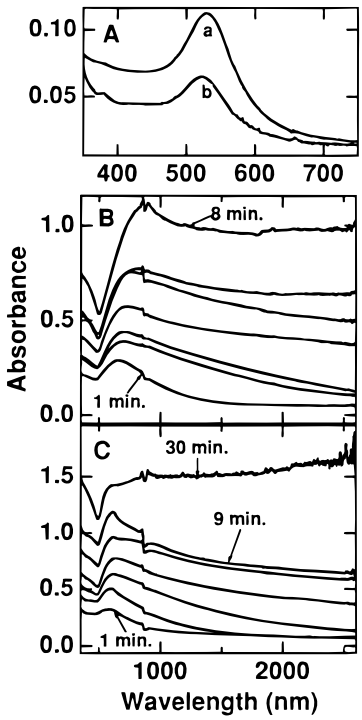


**Figure 2.** (Top panel) Representative optical spectra for 12-nm-diameter Au colloid monolayers on APTMS- (a) and MPTMS-coated glass (b). (Middle panel) UV−vis−near-IR spectra for seven 12-nm-diameter Au colloid monolayers on APTMS/glass after exposure from 1 to 8 min to 0.01% $HAuCl_4$/0.4 mM $NH_2OH$. (Bottom panel) UV−vis−near-IR spectra for seven 12-nm-diameter Au colloid monolayers on MPTMS/glass after exposure from 1 to 30 min to 0.01% $HAuCl_4$/0.4 mM $NH_2OH$.

sions for the particles being interrogated. As time progresses toward 45 min of immersion (bottom panel), extinction of light is large over the entire visible spectrum, including at 526 nm, the position of $\lambda_{max}$ for the monolayer. At longer times, the absorption band broadens considerably and $\lambda_{max}$ gradually shifts past 600 nm; plots of $\lambda_{max}$ vs time (as well as $A_{526}$ vs time) are included in the Supporting Information.

The increase in absorbance accompanying deposition of $Au^0$ onto immobilized colloidal particles extends well into the infrared region of the spectrum. The top panel of Figure 2 shows representative optical spectra from two sets ["high" coverage (a) and "low" coverage (b)] of 20 Au colloid monolayers each from which thin Au films were grown by $Au^{3+}/NH_2OH$ seeding.[24] The middle and bottom panels show near-infrared absorbance over time for Au films grown from colloidal Au monolayers with high and low coverages, respectively. As expected, the absorbance of the low coverage films lags behind that of the high coverage. For example, after 9 min of seeding, the low-coverage sample had an absorbance about 20−25% lower than high-coverage sample exhibited after 8 min.

Although these surfaces comprise only a single layer of particles, as opposed to the numerous strata of spacer-linked colloidal Au in multilayers,[11] they nevertheless exhibit similar near-IR optical spectra. In both cases, increased quantities of Au immobilization lead to decreased transmission and to a loss of wavelength sensitivity. These properties have been observed in percolating Au films prepared by evaporation,[26] with one significant difference: in the latter, the percolation threshold (i.e., the inflection point in insulator−conductor transition) is denoted by the point at which the absorbance becomes wavelength-independent. Here, well before the plots of near-IR absorbance vs wavelength become horizontal, the Au films are very highly conductive. However, evaporated Au films and high-coverage $NH_2OH$-seeded films do share the attribute of increased absorbance at increasing wavelengths (i.e., an upward-sloping line) in the fully metallic regime. Table 1 lists resistance measurements for enlarged low-coverage and high-coverage Au colloid monolayers. Once again, it is clear that bulk properties are reached more rapidly from high coverage surfaces. For example, after 6 min, the resistance of the high-coverage seeded surface is 1/40000th that of the low-coverage seeded surface (14 Ω vs 650 000 Ω). Conversion of measured resistances into resistivities by accounting for measurement geometry) indicates that both seeded films ultimately achieve extraordinarily high conductivies;[27] for low-coverage colloidal Au monolayers immersed in seeding solution for 30 min, the resistivity $\rho = 1.0 \times 10^{-5}$ Ω cm, in comparison with $2.44 \times 10^{-6}$ Ω cm for pure Au at room temperature.[29] Thus, these films are within a factor of

(24) While the high coverage surfaces were on APTMS-functionalized glass and the low coverage surfaces were on MPTMS-coated glass, the differences in coverage do not reflect differences colloidal Au-binding properties of the pendant functional groups, but rather differences in monolayer derivatization time. We have shown else that there are negligible differences in the kinetics or thermodynamics of colloidal Au binding to APTMS or MPTMS.[25] For both sets of surfaces, the standard deviation in absorbance at $\lambda_{max}$ was ±0.004.

(25) (a) Grabar, K. C.; Brown, K. R.; Keating, C. D.; Stranick, S. J.; Tang, S.-L.; Natan, M. J. *Anal. Chem.* **1997**, *69*, 417−477. (b) Bright, R. M.; et al., Submitted for publication. (c) Keating, C. D.; Natan, M. J. Manuscript in preparation.

(26) Smilauer, P. *Contemporary Phys.* **1991**, *32*, 89−102.

**Table 1. Resistance of $Au^{3+}/NH_2OH$−Seeded Au Colloid Monolayers and Multilayers**

| sample | immersion time (min)[a] | resistance (Ω)[b] | corresponding AFM image |
|---|---|---|---|
| low coverage Au monolayer[c] | 1 | insulating | |
| | 3 | insulating | Figure 4, panel B |
| | 6 | 650 000 | Figure 4, panel |
| | 7 | 370 | Figure 4, panel D |
| | 8 | 120 | |
| | 9 | 40 | Figure 4, panel E |
| | 30 | 4 | Figure 4, panel F |
| high coverage Au monolayer[d] | 1 | insulating | |
| | 2 | insulating | Figure 5, panel B |
| | 3 | 1000 | Figure 5, panel C |
| | 4 | 100 | |
| | 5 | 56 | Figure 5, panel D |
| | 6 | 14 | |
| | 8 | 5.6 | Figure 5, panel E |
| | 17 | 0.5 | Figure 5, panel F |
| Au colloid multilayer[e] | 1 | 9 700 000 | |
| | 2 | 6 000 000 | |
| | 4 | 30 000 | |
| | 10 | 40 | |

[a] In a 120 rpm orbital shaker loaded with 0.01% $HAuCl_4$/0.4 mM $NH_2OH$. [b] Direct current resistance as measured with a two-point probe. Measurement length was 2.1 ± 0.1 cm; sample width was 0.9 ± 0.1 cm. [c] 12-nm-diameter Au/MPTMS/glass. [d] 12-nm-diameter Au/MPTMS/glass. [e] 12-nm-diameter Au/MPTMS/glass followed by three treatments each with 2-mercaptoethylamine/17 nM, 12-nm-diameter colloidal Au.

4 of the conductivity of pure Au (of the same thickness), and far exceed the conducitivities for a variety of other metals.

Given the high conductivity of these films, it was reasonable to expect that they could be used as working electrodes in cyclic voltammetry (CV) experiments, an idea supported by the data in Figure 3. The top panel shows cyclic voltammograms for $[Ru(NH_3)_6]^{3+}$ at three different scan rates for a high-coverage, 17-mim seeded Au film. Quasi-reversible voltammetry[30] is obtained, with an $E^{\circ\prime}$ of −0.23 V vs SCE, and peak-to-peak separations ($\Delta E_p$) of 135 mV at 50 mV/s, 180 mV at 100 mV/s, and 210 mV at 200 mV/s. The increase in $\Delta E_p$ with increasing scan rate is indicative of one (or more) barriers to heterogeneous electron transfer (ET), among which could include lack of cleanliness of the electrode, poor ET kinetics at films deposited from solution, or barriers due to complex morphology (vide infra). In any

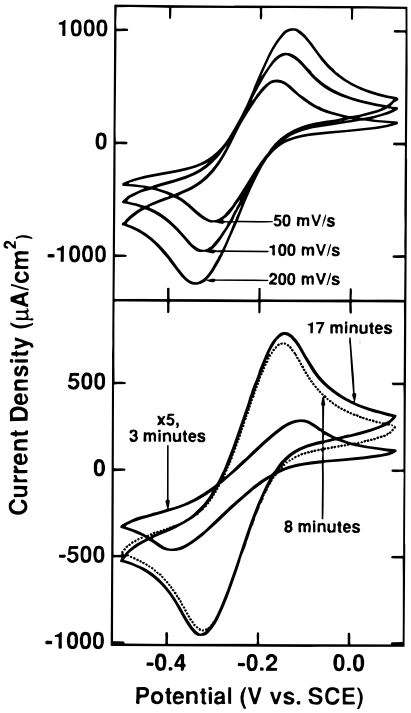


**Figure 3.** (Top) Cyclic voltammograms at three different scan rates of 5 mM $[Ru(NH_3)_6]Cl_3$/0.1 M $Na_2SO_4$ at a colloidal Au film (12-nm-diameter colloidal Au monolayer/APTMS/glass immersed in 0.01% $HAuCl_4$/0.4 mM $NH_2OH$ in an orbital shaker at 120 rpm for 17 min), and (bottom) comparison of 100 mV/s cyclic voltammograms of the same electrolyte taken at colloidal Au monolayers seeded (as above) for 3, 8, and 17 min.

case, there is a clear difference between the highly conductive and partially conductive films (bottom panel): the CV for the Au colloid monolayer immersed for 3 min in to 0.01% $HAuCl_4$/0.4 mM $NH_2OH$, the magnitude of the cathodic current is roughly 10-fold smaller than for the highly conductive films; the broad, drawn-out nature of the CV results in large part from the IR drop across the electrode.

The third set of resistance measurements in Table 1 were made on Au colloid multilayers exposed to 0.01% $HAuCl_4$/0.4 mM $NH_2OH$ for varying lengths of time. From the resistance data and UV−vis−near-IR spectra (Supporting Information), it appears that catalysis of the $Au^{3+} \rightarrow Au^0$ reaction is not facile on colloidal Au particles (at least partially) coated with organic adsorbates such as 2-mercaptoethylamine. Even though the initial, four-layer sample had an absorbance of ∼0.4 (i.e., four times as many particles), the sample resistance is higher per unit time than for the high-coverage Au colloid monolayer. Moreover, although the resistance drops by 5 orders of magnitude, the near-IR absorbance does not become completely wavelength-independent after 10 min of seeding.

Despite these differences, however, the three types of samples discussed in Table 1, namely high- and low-coverage Au colloid monolayers and Au colloid multilayers, all comprise good substrates for $Au^{3+}/NH_2OH$ seeding: all exhibit precipitous decreases in resistance, and all take on bulk optical properties in the near-IR similar to those exhibited by evaporated Au films.

**Film Nanostructure by AFM and FE-SEM.** While the bulk measurements described above certainly pro-

(27) Resistivity ($\rho$) is calculated using the formula $\rho = RAL^{-1}$, where $R$ is the measured resistance in ohms, $A$ is cross-sectional area, and $L$ is the length over which $R$ is measured. From data in Figures 4 and 5 and the Supporting Information, the upper limit to film thickness (for samples with low coverage of colloidal Au) is 50−60 nm; the average thickness is actually lower. Thus, $A = 0.9 \times (60 \times 10^{-7}) = 5.4 \times 10^{-6}$ cm$^2$. Using the lowest value for $R$ for the low-coverage colloidal Au film (4 Ω) and $L$ = 2.1 cm from Table 1, $\rho_{\text{seed film}} = 1.0 \times 10^{-5}$ Ω cm. Note that unambiguous, quantitative measurements of the quantity of Au in a film can be made by digestion of the surface and subsequent analysis of Au using atomic absorption. These measurements gave a film thickness of 70 nm for the thickest film.[28]

(28) The deposition rate for $Au^0$ was linear over time (Supporting Information). Samples treated with 0.01% $HAuCl_4$/0.4 mM $NH_2OH$ for 1, 3, 5, 7, 9, 11, 15, and 30 min were found to contain 300, 548, 913, 1185, 1241, 1612, 1684, and 3628 ppb, respectively. By using the 6-mm O-ring, 0.283 cm$^2$ of surface film was removed. If the film was 35 nm thick this would produce a (cylindrical) volume of $0.991 \times 10^{-6}$ cm$^3$. From the density of Au (19.3 g/cm$^3$), 19.1 μg of Au would be dissoved. When taken up in 10 mL, the solution concentration is 1.9 ppm. Since the 30-min sample was found to contain 3.6 ppm, it means that the equivalent of a 66-nm-thick Au film had been removed.

(29) Weast, R. C., Ed. *CRC Handbook of Chemistry and Physics*, 69th ed.; CRC Press Inc.: New York, 1988; p E-93.

(30) Bard, A. J.; Faulkner, L. R. Electrochemical Methods; John Wiley and Sons: New York, 1980; pp 213−248.

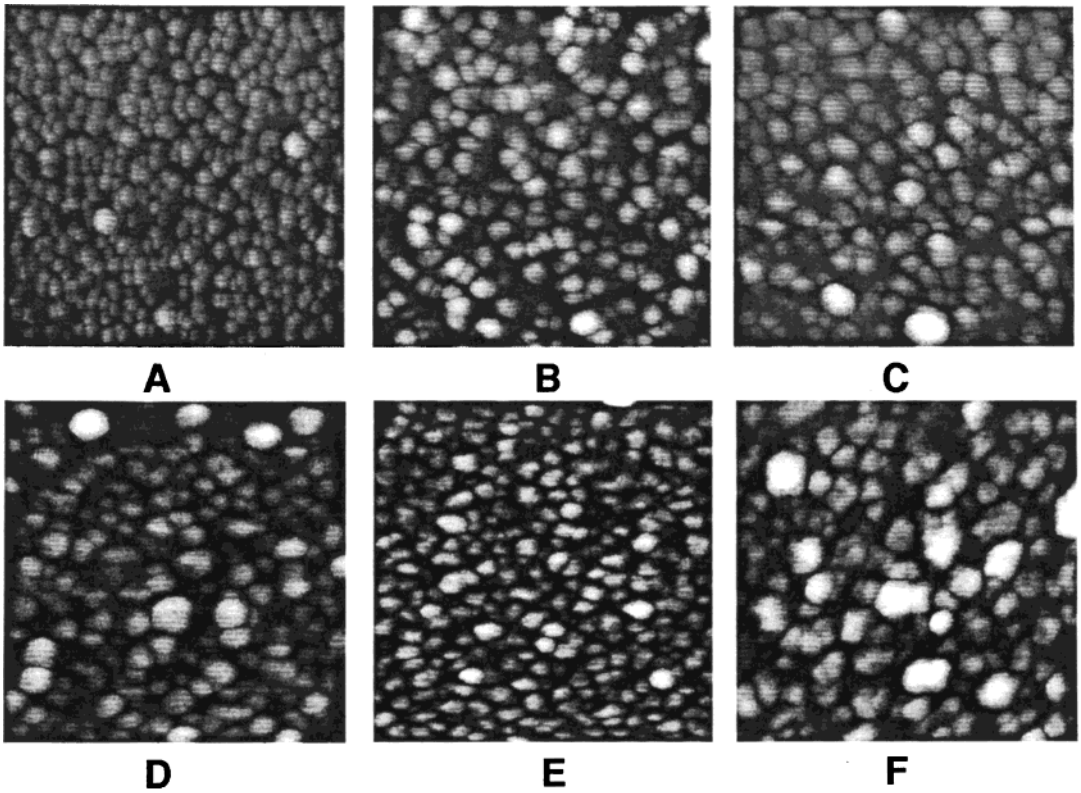


**Figure 4.** AFM images (1 $\mu$m × 1 $\mu$m) of a 12-nm-diameter Au colloid monolayer on MPTMS-coated glass (A), and after shaking in an orbital shaker at 120 rpm in a solution of 0.01% $HAuCl_4$/0.4 mM $NH_2OH$ for 3 (B), 6 (C), 7 (D), 9 (E), and 30 min (F).

vide sufficient evidence that immobilized Au nanoparticles can be enlarged by $Au^{3+}/NH_2OH$ seeding, they do not provide the information on particle size and shape that is necessary for comparison of surface and solution processes. Likewise, while near-IR and resistance data clearly established differences in the approach to metallic behavior for Au colloid monolayers with high and low particle coverages, they do not yield any insight into the actual mechanism of particle coalescence. Both these issues can be resolved by a combination of AFM and FE-SEM analysis. As elaborated more fully elsewhere,[25a] both types of measurements are essential, since only FE-SEM reveals the true particle positions and dimensions in the $x-y$ plane, and only AFM can measure film thicknesses in the $z$ direction.

The time course of $Au^{3+}/NH_2OH$-mediated enlargement of immobilized Au nanoparticles at low coverage and at high coverage are revealed by AFM images in Figures 4 and 5, respectively. Each figure is made up of six images, starting with the monolayer (A), and follows the evolution of highly conductive films over the last five images (B−F). For each, the latter five images were acquired from the same samples from which resistance data were obtained (Table 1). For each image, the $z$-scale covers 50 nm, with the dark pixels being lower and the white pixels being higher; AFM line scans for each of the 12 images presented in Figures 4 and 5 can be found in the Supporting Information. To be certain that acquired images were not anomalies, the Supporting Information also contains four additional AFM images for each image in both figures.

The AFM image of the low-coverage Au colloid monolayer (Figure 4, panel A) shows individual particles between 12 and 15 nm in height and with flat spaces in between. The corresponding panel in Figure 5 shows a close-packed arrangement of particles. In point of fact, this is an artifact of AFM tip convolution on these samples—previous FE-SEM and TEM data have conclusively shown that images such as these correspond to 0.2−0.3 monolayers.[15,22,25] Nevertheless, the two images provide a clear view of the differences in initial particle coverage.

For the low-coverage film, $Au^{3+}/NH_2OH$ seeding leads to evolution of features that are both taller and broader. The line scan corresponding to panel F in Figure 4 shows features as tall as 50 nm and as wide as 75 nm (the line scan indicates a width of ∼150 nm, but true particle dimensions in the $x-y$ plane are actually only about half those recorded[15,22,25]). Moreover, the features are substantially closer together than the original features imaged on the colloidal monolayer. Because of AFM tip convolution, it is impossible to determine interparticle spacing, but it is worth noting that the samples corresponding to images D, E, and certainly F conduct electricity (Table 1). Therefore, there must be extensive domains where particles are in contact or are close enough to each other to allow efficient electron tunneling.[31] AFM tip convolution also prevents calculation of the particle ellipticity $G$ (the ratio of major:minor axis; $G = 1$ for a sphere), but there appear to be none of the high-aspect ratio rod-shaped particles synthesized during $Au^{3+}/NH_2OH$ seeding in solution.[5]

$Au^{3+}/NH_2OH$ seeding on the high-coverage Au colloid monolayer (Figure 5) follows a different pattern than that described for the low-coverage sample (Figure 4). While comparison of panels A and F clearly indicate an

(31) Adkins, C. J. In *Metal−Insulator Transitions Revisited*; Edwards, P. P., Rao, C. N. R., Eds.; Taylor and Francis: London, 1995; pp 191−210 and references therein.

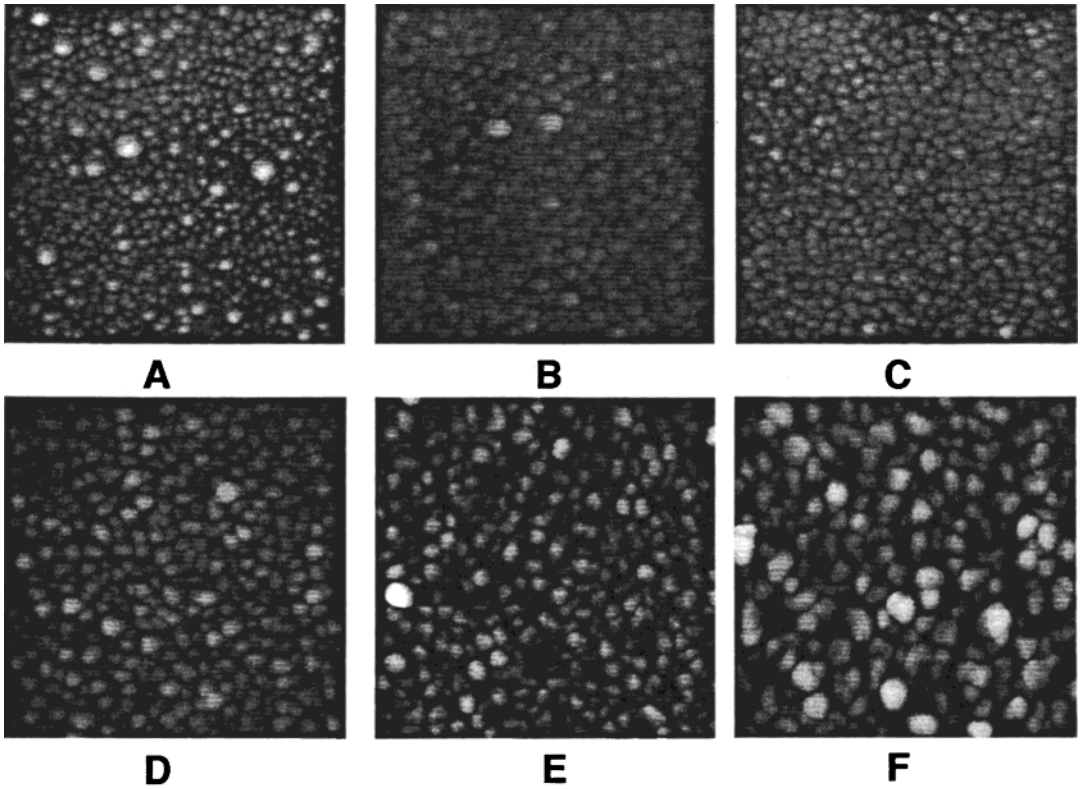


**Figure 5.** AFM images (1 $\mu$m × 1 $\mu$m) of a 12-nm-diameter Au colloid monolayer on APTMS-coated glass (A), and after shaking in an orbital shaker at 120 rpm in a solution of 0.01% $HAuCl_4$/0.4 mM $NH_2OH$ for 2 (B), 3 (C), 5 (D), 8 (E), and 17 min (F).

increase in both particle height and width, neither is as dramatic as seen for the low-coverage film. For example, the largest features for the sample imaged in Figure 5, panel F (high coverage, 17-min seeding) and the accompanying Supporting Information is ~25 nm, compared to ~50 nm for the sample imaged in Figure 4, panel F (low coverage, 30-min seeding) and the accompanying Supporting Information. At earlier times, the high coverage surface appears even flatter: the most prominent vertical features in line scans of panels B, C, and D of Figure 5 are less than 18 nm high.

One explanation for the decreased film thickness for the high-coverage monolayer is that particle coalescence occurs at an earlier stage of seeding. In other words, if $Au^0$ is preferentially deposited between Au nanoparticles, then growth occurs in the $x-y$ plane at a greater rate than on the $z$ axis. Such a model would explain the early-time conductivity of the high coverage sample. For instance, the five images of the sample seeded for 3 min (Panel C of Figure 5 and Supporting Information) are remarkably absent of large vertical features, and all have a higher density of curved features in the plane than previously imaged Au colloid monolayers, for which each feature could be identified by transmission electron microscopy or FE-SEM as an individual colloidal particle.[15,22,25] Since new particle nucleation is ruled out on this time scale,[5] the additional curved features must be associated with the original particles, suggesting a highly complex particle morphology.

This hypothesis is substantiated by the FE-SEM data in Figure 6, which shows images corresponding to C and F from Figure 4 (panels B and D, respectively), as well as C and F from Figure 5 (panels A and C, respectively). After 3 min of immersion in $Au^{3+}/NH_2OH$, the high-coverage surfaces exhibit an extraordinarily complex nanostructure (panel A).[32] Not only has extensive particle fusion taken place, differential growth rates in the same direction from different parts of fused particles has led to production of 3-D objects that are impossible to describe as linear combinations of spheres and/or rods (or any other regular shape, for that matter). In short, the nanostructure is now indistinguishable from those of granular metal films prepared by evaporation. Indeed, the mean roughness of this sample is only 3-nm rms, the same value obtained via a morphological analysis of discontinuous metal films prepared by evaporation at ultrahigh vacuum.[33,34]

Short-time seeding of low-coverage Au colloid monolayers leads to a startlingly different (but expected) nanostructure (Figure 6, panel B): after 6 min, there is little particle fusion. To the contrary, a collection of isolated larger particles is seen, many of which are elliptically shaped. Also, about 10−15% of the particles are isolated spheres of 40−50 nm diameter. Clearly, increasing the interparticle spacing promotes "solution-like" enlargement, and notwithstanding the fused particles, the resulting surface looks like one that might obtained by self-assembly of a 50-nm-diameter colloidal Au particles prepared by the Frens method.[7]

FE-SEM images of Au films derived from prolonged $Au^{3+}/NH_2OH$ seeding of high-coverage and low-coverage Au colloid monolayers (panels C and D, respectively, of Figure 6) are far more similar than their predecessors.

(32) Note that because of in-lens detection used in data acquisition with the JEOL 6320F, no sample coating is needed, so the image represents the actual nanostructure.

(33) Blacher, S.; Brouers, F.; Gadenne, P.; Lafait, J. *J. Appl. Phys.* **1993**, *74*, 207−213.

(34) A 5 $\mu$m × 5 $\mu$m scan of the surface imaged in Figure 5, panel F gave an rms roughness for the entire 25 $\mu m^2$ surface of 6 nm.

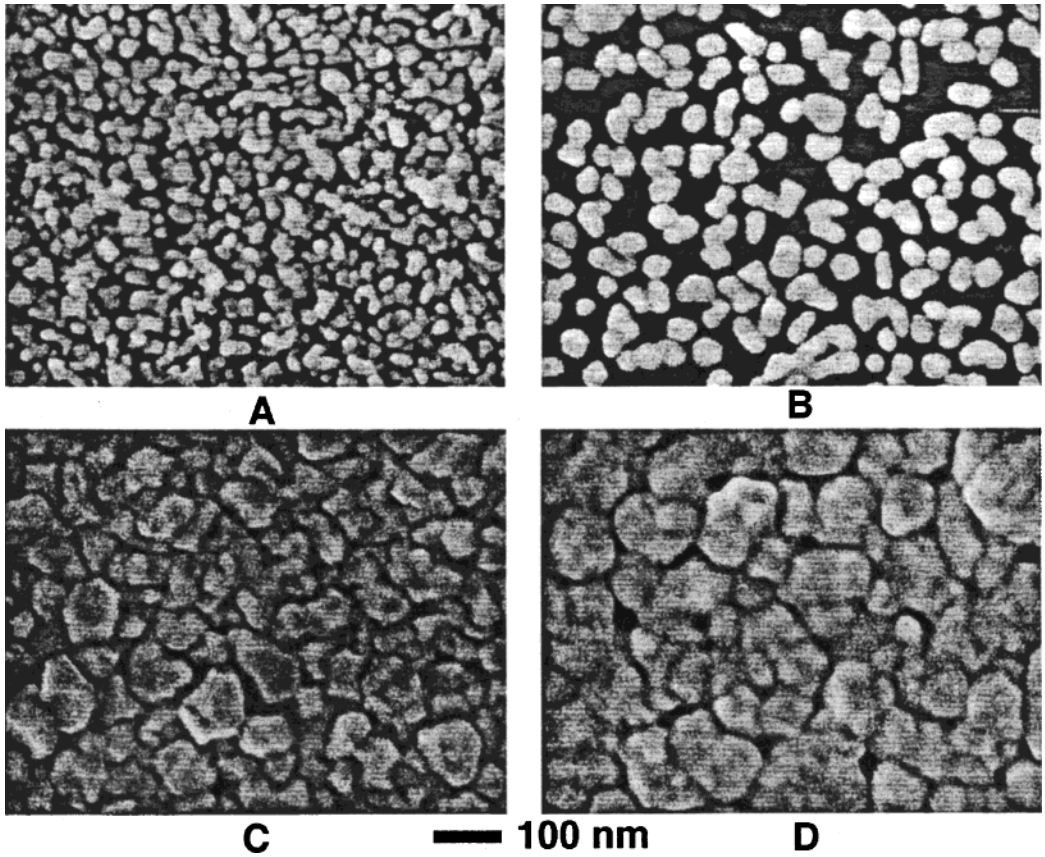


**Figure 6.** FE-SEM images of $Au^{3+}/NH_2OH$-enlarged Au colloid monolayers. Images A and C correspond to samples imaged by AFM in Figure 5, panels C and F, respectively; images B and D correspond to samples imaged by AFM in Figure 4, panels C and F, respectively.

Both films exhibit large-scale particle fusion, with all vestiges of the original nanostructure completely obscured. The only discernible difference between the samples is the presence of scattered "holes" in the low-coverage film, likely a product of incomplete coalescence of large particles.

The images in Figures 4−6 reveal how two very different growth mechanisms can yield equally conductive surfaces by $Au^{3+}/NH_2OH$ seeding: at high coverages, early-time coalescence of smaller particles leads to a granular film, while at low coverage, isolated particles are seeded to form distinct, larger particles prior to their ultimate fusion.

**Nanometer-Scale Optical Properties.** The low transmittance of metallic Au/air interface in the near-IR (Figure 2) is an intrinsic optical property of Au that depends solely on its wavelength-dependent dielectric properties.[35] In contrast, several optical properties of Au depend on nanostructure, including SERS,[13] SPR,[18] and nonlinear optical behavior.[36] Accordingly, we sought to investigate the effects of particle enlargement and surface roughening via $Au^{3+}/NH_2OH$ seeding on these optical phenomena.

Figure 7 shows SERS spectra for 10 mM solutions of BPE drop-coated onto a 12-nm-diameter colloidal Au/APTMS/glass substrate (a) and onto identical substrates after immersion in 0.01% $HAuCl_4$/0.4 mM $NH_2OH$ for 1 (b), 6 (c), and 17 min (d). Seeding leads to significant increases in signal (∼50) compared to the relatively weakly enhancing Au colloid monolayer. Such changes are reminiscent of those occurring upon deposition of a Ag cladding on colloidal Au arrays.[37] However, the

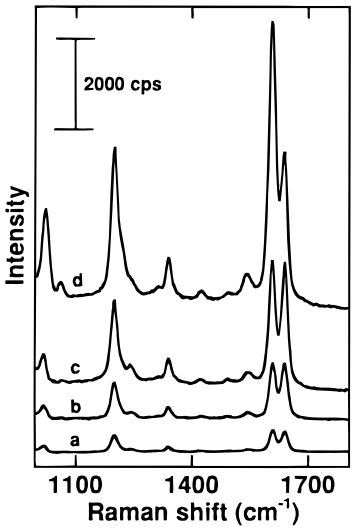


**Figure 7.** SERS spectra of 10 mM BPE in 9:1 $H_2O$:$CH_3OH$ drop-coated on 12-nm-diameter Au colloid monolayers on APTMS-coated glass as prepared (a) and after exposure to 0.01% $HAuCl_4$/0.4 mM $NH_2OH$ for 1 (b), 6 (c), and 17 min (d). Acquisition parameters: 23 mW of 632.8-nm photons at the sample; integration time = 1 s; ∼8 $cm^{-1}$ band-pass.

(35) Optical Properties of Thin metal Films book.

(36) (a) Fukumi, K.; Chayahara, A.; Kadono, K.; Sakaguchi, T.; Horino, Y.; Miya, M.; Fujii, K.; Hayakawa, J.; Satou, M. *J. Appl. Phys.* **1994**, *75*, 3075−3080. (b) Hache, F.; Richard, D.; Flytzanis, C. *J. Opt. Soc. Am. B* **1986**, *3*, 1647−1655.

(37) Baker, B. E.; Kline, N. J.; Treado, P. J.; Natan, M. J. *J. Am. Chem. Soc.* **1996**, *118*, 8721−8722.

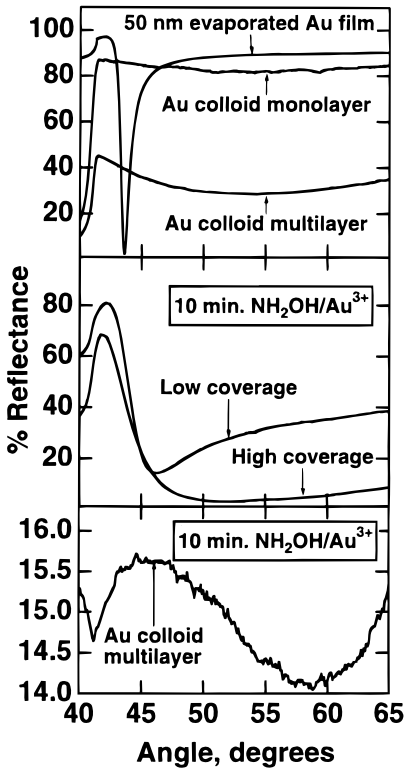


**Figure 8.** (Top panel) Simulated SPR curve for a 50-nm-thick evaporated Au film on glass and observed SPR curves for a 12-nm-diameter Au colloid monolayer/APTMS/glass substate and a 12-nm-diameter Au colloid multilayer substrate (Au colloid monolayer on MPTMS-coated glass with seven additional colloidal layers added using 2-mercaptoethylamine as a bifunctional cross-linker[11]). (Middle panel) SPR curves for high and low coverage 12-nm-diameter Au colloid monolayers on organosilane-coated glass after 10 min of shaking in an orbital shaker (at 120 rpm) in a solution of 0.01% $HAuCl_4$/0.4 mM $NH_2OH$. (Bottom panel) SPR curve for the Au colloid multilayer of the top panel after the $HAuCl_4/NH_2OH$ treatment described for the middle panel.

increases in signal for Ag−rclad Au were sufficiently large (i.e., ×1000) to be unexplainable by anything other than electromagnetic effects. Here, it is unclear whether the increased SERS intensity reflects increased surface area, nanometer-scale changes in optical properties, a change in orientation of adsorbed BPE (note the change in intensity ratio for the ring-breathing modes[38] at 1607 and 1640 $cm^{-1}$), or a combination of the effects. Deconvolution of these effects is beyond the scope of this work; it suffices to point out that these surfaces give SERS enhancements equivalent to surfaces prepared by more effort-intensive (and expensive) methods as evaporation or sputtering.[39]

While SERS is extraordinarily sensitive to nanostructure at the surfaces of free electron metals such as Au, it is a rather poor probe of *interior* nanostructure, as long as it does not impact bulk optical properties. In contrast, SPR depends on propagation of surface plasmons through thin Au films on glass substrates under conditions of total internal reflection. Since the plasmons are launched by evanescent waves that penetrate

(38) McMahon, J. J.; Babcock, G. T. *Spectrochim. Acta* **1982**, *38A*, 1115−1122.

(39) (a) Semin, D. J.; Rowlen, K. L. *Anal. Chem.* **1994**, *66*, 4324−4331. (b) Maya, J. L.; Vallet, C. E.; Lee, Y. H. *J. Vac. Sci. Technol. B* **1997**, *15*, 238−242.

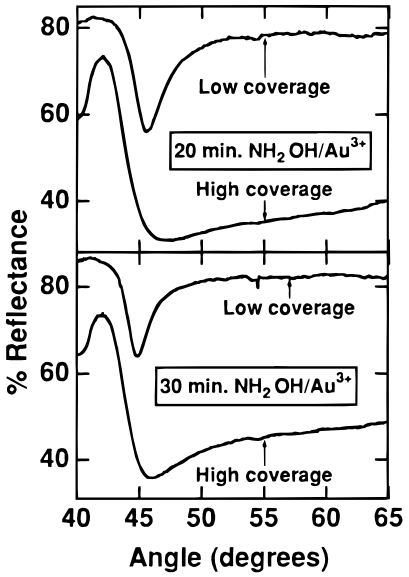


**Figure 9.** SPR curves for high and low coverage Au colloid monolayers on organosilane-coated glass substrates after 20- and 30-mim exposures to the seeding solution as described in Figure 8.

the Au to a depth of ∼150 nm, internal film structure is critical.

Figure 8 shows the variety of SPR responses that can be obtained with evaporated and colloidal Au films. The top panel shows simulated reflectance vs excitation angle curves for a 50-nm-thick evaporated Au film, and experimental data for a 12-nm-diameter colloidal Au/APTMS/glass surface and an eight-layer 12-nm-diameter Au colloid multilayer. While the evaporated films shows a sharp minimum in reflectivity that comprises the basis for biological applications of SPR,[19] both the Au colloid monolayer and multilayer exhibit broad reflectivity profiles. For the monolayer, the high reflectivity is due to the low sample absorbance at 632.8 nm; the large extinction of the multilayer at this wavelength leads to low reflectivity.

Particle enlargement and/or coalescence by $NH_2OH$ seeding leads to increased definition in SPR reflectivity curves for low- and high-coverage Au colloid monolayers (middle panel) as well as for Au colloid multilayers (bottom panel). For the latter, after a 10-min immersion in the seeding bath, there is a further decrease in reflectivity, with concomitant evolution of fine structure. In particular, there is a spike at ∼41°, and a sinusoidal variation in reflectivity from 45° to 65°. Changes in reflectivity at the former (the critical angle) are expected; the origin of the latter feature is unknown, but clearly results from changes in film morphology.

Of greater interest are the changes in the monolayer reflectivity after a 10-min immersion in $Au^{3+}/NH_2OH$. For the high-coverage surface, there is now a broad minimum in reflectivity that only slowly dissipates over 20+°. The low-coverage surface shares a similar profile, but minimum is less shallow. This difference is magnified at 20- and 30-min immersion times (Figure 9). In general, there is an increase in reflectivity, as expected with 632-nm excitation for Au films that are greater than 50 nm thick.[18] More importantly, while the minimum in reflectivity for the high coverage film is only slightly more pronounced than for a 10-min immersion,

a clean, relatively narrow minimum has evolved on the low-coverage surface. It is surprising that the SPR signature is so dramatically distinct for two films that have the same conductivity (Table 1), the same optical spectrum (Figure 2), and an almost identical nanostructure (panels C and D of Figure 6); at the same time, although, it is reasonable to expect that the SPR response, which is ideal for a 50-nm-thick Au film with 3−4-nm roughness, would be better on the low-coverage film, in which particle growth proceeded prior to roughly 40−45 nm in diameter prior to coalescence. If this hypothesis is true, it suggests that $Au^{3+}/NH_2OH$ seeding of Au colloid monolayers with even lower coverages would lead to sharper SPR curves, via growth of isolated particles to even larger dimensions before fusion.

## Conclusions and Summary

$Au^{3+}/NH_2OH$ seeding of colloidal Au films provides entry to a series of complex Au nanostructures that have been probed by UV−vis−near-IR, electrochemistry, resistance measurements, atomic absorption, AFM, FE-SEM, SERS, and SPR. For colloidal Au multilayers linked by 2-mercaptoethylamine, particle enlargement proceeds with the expected consequences, namely increased UV−vis−near-IR extinction, and decreased in resistance and reflectivity. The behavior of Au colloid monolayers depends markedly on particle coverage. At high coverage, seeding leads to early particle coalescence, resulting in films indistinguishable from those prepared by evaporation of Au onto thiol-terminated glass substrates (which is widely used to promote Au adhesion). Indeed, seeding of high-coverage Au colloid monolayers can be considered a vacuum-free route to production thin films remarkably similar to those produced by evaporation. At low coverage, the isolated particles grow individually into spheres, rods, and ellipses, in analogy to the process in solution. Continued growth leads to conductive films whose reflectivity vs excitation-angle curves exhibits pronounced minima. Once again, this property resembles that of evaporated Au flims of narrowly defined specfications that are used for SPR experiments. These data suggest that $Au^{3+}/NH_2OH$ seeding is a valuable tool in Au surface nanoarchitecture; further studies of its utility are underway.

**Acknowledgment.** Support from NSF (CHE-9256692, CHE-9627338), NIH (GM55312-01), and the Sloan Foundation is gratefully acknowledged. Acknowledgment is also made to the Electron Microscopy Facility for the Life Sciences in the Biotechnology Institute at The Pennsylvania State University.

**Supporting Information Available:** Time dependence of $A_{526}$ and $\lambda_{max}$ for seeding on a 12-nm-diameter Au colloid monolayer, UV−vis−near-IR spectra for seeded Au colloid multilayers, plot of atomic absorption-derived Au mass vs immersion time, line scans, and four additional AFM images for each image shown in Figures 4 and 5, and FE-SEM data for the high-coverage Au colloid monolayer. This material is available free of charge via the Internet at http://pubs.acs.org.

CM980066H